Research Article Open Access

Yi Qian*, Kangjia Jiang and Long Li*

Improving the flame retardancy of ethylene vinyl acetate composites by incorporating layered double hydroxides based on Bayer red mud

https://doi.org/10.1515/epoly-2019-0015
Received August 02, 2018; accepted October 07, 2018.

Abstract: Nowadays, reducing the hazards of bayer red mud (BRM) is an important research direction in the fields of environmental and safety. In this article, Mg/Al/Fe ternary layered double hydroxides (Mg/Al/Fe-LDHs) were synthesized successfully by a co-precipitation method based on introducing Mg^{2+} into the BRM suspension. The thermogravimetric analysis (TGA) results showed that the decomposition rate of LDHs is higher than that of BRM, which indicates that LDHs can absorb more heat than BRM during the decomposition process. Subsequently, BRM and LDHs were added into the ethylene vinyl acetate (EVA) to investigate its effects on reducing flammability of the composites. The cone calorimeter test (CCT) results demonstrated that 50 wt% LDH-B can make the peak value of HRR (PHRR) decrease from 1694.8 kW/m^2 (EVA) to 199.2 kW/m^2 (ELDH2). The smoke density test (SDT) results showed that the luminous flux of ELDH2 is nearly 95% at the end of test with a pilot flame, which is much higher than that of EVA and EBRM. The thermogravimetry-Fourier transform infrared spectrometry (TG-FTIR) results confirmed that LDHs can improve the thermal stability of composites and reduce the production of some toxic gases. Compared with BRM, the improved flame retardancy of Mg/Al/Fe-LDHs is ascribed to the introduction of Mg^{2+}, which offering an enhanced catalytic carbonization capability, as well as the physical barrier effect of char residue layer catalyzed by the lamellar LDHs.

Keywords: bayer red mud; layered double hydroxides; co-precipitation; ethylene vinyl acetate; flame retardancy

*** Corresponding authors: Yi Qian and Long Li,** College of Environment and Safety Engineering, Qingdao University of Science and Technology, Qingdao, Shandong 266042, P R China, email: qianyi1962@126.com (Yi Qian); lli@yic.ac.cn (Long Li).
Kangjia Jiang, College of Environment and Safety Engineering, Qingdao University of Science and Technology, Qingdao, Shandong 266042, P R China.

1 Introduction

Ethylene vinyl acetate (EVA) copolymer as a universal engineering material is widely used in all aspects of human production and life (1-3). However, potential fire hazards associated with the use of the EVA, such as high heat and dense smoke generation as well as some toxic gases release during combustion, which may seriously threaten human survival and greatly limited its widespread applications, especially in high temperature service conditions (4,5).

Recently, to improve the flame retardancy and smoke suppression performance, great interests in developing flame retardant EVA composites have been significantly growing, introducing flame retardants into EVA is the most convenient and economical method (6-8). Due to corrosiveness and environmental concerns, halogen-containing additives are severely restricted and halogen-free flame retardants have become the focus of attention (9), such as metal hydroxides (10,11), expandable graphite (12) and carbon nanotubes (6,13,14). In recent years, layered double hydroxides (LDHs) have been extensively studied as flame retardant for EVA and shown excellent flame retardant effect (4,15).

Layered double hydroxides, also known as anionic clays (16-18). The general chemical formula of LDHs is $[M(\mathrm{II})_{1-x}M(\mathrm{III})_x(OH)_2]^{x+}(Y^{m-})_{x/m}\cdot nH_2O$, M(II) and M(III) are bivalent and trivalent cations, and Y stands for m valence inorganic or organic acid anions. Inorganic hydrotalcites are widely used as heterogeneous catalysis, adsorbents, electrochemicals, and flame-retardant additives in polymeric materials (3,19). Gao and his colleagues have demonstrated that the PHRR of HDPE was significantly reduced with incorporation of the LDHs with different interlayer inorganic ions, this can be attributed to the physical barrier formed on the surface of the sample, which slows down heat transfer and prevents the matrix material from further pyrolysis

and combustion (20). Yan et al reported that the peak of smoke production rate and peak of CO release rate of PS/LDHs nanocomposites were reduced significantly comparing with pure PS phase (21).

Bayer red mud (BRM), as a by-product of alumina production from bauxite by the Bayer process, also called bauxite residue (22). Globally, the increase in demand for alumina has led to an increase in the production of BRM. Nowadays, the cumulative storage of BRM exceeds more than 4 billion tons and is still growing rapidly, which requires a safe disposal, otherwise it may cause serious environmental pollution. BRM dry mass contains large amounts of metal oxides, such as Fe_2O_3 (ca. 41%), Al_2O_3 (ca. 17%) and TiO_2 (ca. 9%), etc. Comprehensive utilization of bayer red mud is cost-effective, however, as a kind of recyclable resources, there are few other effective alternatives to landfill (23). In the past few decades, several methods have been adopted and been practiced all over the world for the processing of bauxite residue, numerous publications have demonstrated that the bauxite residue can be used as an adsorbent to sequester carbon dioxide (24), to remove phosphate (25) and fluoride (26) from water, and obtained rare earth metals by leaching experiments (22,27). These methods can solve the problem of cumulative storage of BRM to a certain extent, nevertheless, when bauxite residue was used to reduce environmental pollution, the risks imposed by the BRM itselves cannot be ignored, for example, it may cause secondary pollution.

Therefore, to successfully transform bauxite residue from a waste to a new product, we need to focus on the performance, cost, and risks. Since BRM contains Al and Fe elements, it could be used to prepare the LDHs. There are many studies on the preparation of LDHs, but few have used an industrial waste such as BRM as a raw material. Our previous work have confirmed that LDHs can be synthesized by a calcination-rehydration method based on BRM, and showed obviously enhance the flame-retardant properties of EVA composites (28-30). However, calcination-rehydration method requires harsh high temperature conditions. In this paper, we further explore the novel mild method, co-precipitation method, to prepare Mg/Al/Fe-LDHs based on introducing Mg^{2+} into the BRM suspension. The XRD results confirmed that LDHs were synthesized successfully, and TGA results showed that the decomposition rate of LDHs is higher than that of BRM. Moreover, the properties of flame retardancy, smoke suppression and thermal stability in EVA have been investigated by CCT, LOI, SDT and TG-FTIR, and we simply explain the mechanism of flame retardancy.

2 Experimental

2.1 Materials

EVA copolymer containing 18 wt% vinyl acetate was purchased from Beijing Eastern Petrochemical Co., Ltd. China. Hydrochloric acid (HCl, 36%), sodium hydroxide (NaOH), sodium carbonate (Na_2CO_3) were obtained from Tianjin Bodi Chemical Reagent Co., Ltd. China. $MgCl_2{\cdot}6H_2O$ was purchased from Sinopharm Chemical Reagent Co., Ltd. China. All above chemicals used in the preparation were analytical grade without further purification. BRM was sponsored by Aluminum Corporation of China Shandong Branch. According to previous research, the element composition and content of BRM are O (37.12%), Fe (35.61%), Al (11.33%), Na (7.11%), Si (5.16%), Ti (2.15%), Ca (0.62%), Co (0.5%) and S (0.4%) (17). BRM was dried at 105°C for 24 h and calcined at 650°C for 4 h, then grinded and sieved before use.

2.2 Synthesis of Mg/Al/Fe-LDHs

LDHs were synthesized through a co-precipitation method: 10 g of BRM powder was poured in 25 mL deionized water solution, and 25 mL of 36% HCl was added. The mixture was kept for digestion at 90°C for 1.5 h. Then $MgCl_2{\cdot}6H_2O$ was added into the solution with [Mg]/[Al + Fe] molar ratios of 1.0/1.0 (LDH-A), 2.0/1.0 (LDH-B), 3.0/1.0 (LDH-C), 4.0/1.0 (LDH-D), and 5.0/1.0 (LDH-E). The above solution was dropped slowly into 200 mL of deionized water. Then, the pH of the mixture solution was adjusted to a range of 8.5-9.5 using NaOH-Na_2CO_3 mixture (1 M NaOH and 0.4 M Na_2CO_3) with rapid stirring. The slurry was then aged for 8 h at 80°C. Finally, the product was filtered, washed to nearly neutral and dried at 80°C for 12 h.

2.3 Preparation of EVA/LDHs composites

Pure EVA and its composites were prepared through the melt blending method using an internal mixer with a rotor speed of 30 rpm. The temperature and time of the internal mixer were set at 120°C and 600 s, respectively. Then, the mixtures were hot

pressed into sheets under 10 MPa at 120°C for 600 s. The sheets were cut into suitably sized samples according to the requirements of measurements. In this paper, all composites were filled with 50 wt% nanoparticles excepting pure EVA. The samples were named EBRM, ELDH1, ELDH2, ELDH3, ELDH4 and ELDH5, which containing 50 wt% BRM, LDH-A, LDH-B, LDH-C, LDH-D and LDH-E, respectively.

2.4 Measurements

2.4.1 X-ray diffraction (XRD)

XRD patterns were obtained by using a Philips *X'*Pert Pro Super apparatus (Nicolet Instrument Co., Madison, WI) equipped with a Cu-Kα tube and Ni filter (λ= 0.1542 nm).

2.4.2 Thermogravimetry–Fourier transform infrared spectrometry (TG-FTIR)

TG-FTIR of the samples were carried out using a TG209 F1 (Netzsch Instruments, Germany) thermogravimeter that was interfaced to the Vertex70 FTIR (Bruker Optics, Germany) spectrophotometer. Each sample (about 10.0 mg) was put in an alumina crucible and heated from room temperature (30°C) to 700°C at a linear heating rate of 20°C/min, nitrogen flow rate was set at 30 mL/min.

2.4.3 Scanning electron microscopy (SEM)

Scanning electron micrographs were obtained by using a Hitachi X650 equipment (Japan) with an acceleration voltage of 8 kV.

2.4.4 Transmission electron microscopy (TEM)

Transmission electron microscope was carried out using a JEM-2100EX equipment (Japan) with an acceleration voltage of 100 kV.

2.4.5 Cone calorimeter test (CCT)

The combustion performance of EVA composites was carried out using a cone calorimeter performed in the Stanton Redcroft device (UK) according to the ISO 5660 standard procedures with an external heat flux of 50 kW/m^2. The samples with the dimensions of $100 \times 100 \times 4$ mm^3 was wrapped in aluminum foil.

2.4.6 Limiting calorimeter test

The LOI values were measured on an HC-2 oxygen index instrument (China) according to ASTM D2863-97. The dimensions of the samples were $100 \times 6.5 \times 3$ mm^3 and the LOI value was the average of five experiments.

2.4.7 Smoke density test (SDT)

Smoke density tests were performed with a JQMY-2 SDT instrument (Jianqiao Co., Ltd. China) according to ISO 5659-2. The dimensions of the samples were $75 \times 75 \times 3$ mm^3 and wrapped in aluminum foil. Experiments were carried out under a heat radiation of 25 kW/m^2 without or with the application of a pilot flame.

3 Results and discussion

3.1 XRD characterization of BRM and LDHs

The XRD patterns of BRM and Mg/Al/Fe-LDHs are displayed in Figure 1. The typical diffraction peaks of all LDHs materials at nearly 11.4°, 22.5° and 35.5° are ascribed to the (0 0 3), (0 0 6) and (0 0 9) planes, respectively. Calculated from the (0 0 3) plane, the interlayer spacing of LDHs is 0.78 nm, indicating the intercalation of CO_3^{2-} ions into the interlayer spaces, which matches the value for Mg/Al/Fe-LDHs reported in the literature (31). Obviously, the diffraction peak of BRM is different from that of LDHs. These results indicated that LDHs can be synthesized after

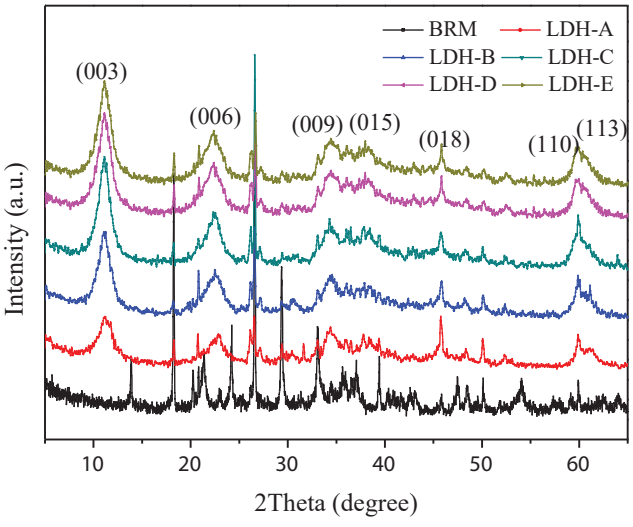

Figure 1: XRD patterns of BRM and Mg/Al/Fe-LDHs.

the introduction of Mg^{2+} into the BRM suspension. The reason is that with the introduction of Mg^{2+}, the number of cations increases, and the negative charge of CO_3^- and OH^- balances with the positive charge, so LDHs were synthesized successfully by a co-precipitation method in alkaline system.

3.2 Thermal stability of BRM and LDHs

The thermal stability of BRM and LDHs were investigated by TGA and differential thermogravimetry (DTG) under a nitrogen flow at a linear heating rate of 20°C/min. The TGA and DTG curves are given in Figure 2. It can be seen from Figure 2a that all curves show two-step thermal degradation, depicting two-stage degradation processes in the range of 50-700°C. The temperature of maximum degradation for each step is taken as T_{max}. From Figure 2b, the first step of BRM appears below 200°C is likely to correspond to the loss of adsorbed water molecules, with the T_{max} is 143.4°C. While the second step starts above 200°C involves the thermal decomposition of metal oxides and the T_{max} at this step is 293.4°C. Meanwhile, the first weight loss of LDHs occur at about 50-250°C due to the removal of interlayer water, the weight loss of LDH-(A~E) are 9.2%, 11.5%, 12.8%, 11.9% and 13.5%, and the T_{max} are 166°C, 165°C, 169°C, 170°C and 159°C, respectively. The second weight loss occur at about 250-700°C due to the elimination of the structural water in the layers and interlayer anions, which leads to breaking of the layer structures, as reported in the literatures (32). The weight loss of LDH-(A~E) are 26.6%, 32.4%, 38.6%, 36.4% and 38.9%, and the T_{max} are 349°C, 347°C, 360°C, 381°C and 383°C, respectively. In addition, it is worth noticing that BRM leaves more residue compared to LDHs at the end of the TGA test, meaning that the decomposition rate of LDHs is higher than that of BRM. The decomposition rate has a positive correlation with the absorbed heat value during the decomposition process, so the high decomposition rate indicates that LDHs can absorb more heat than BRM. Additionally, it can be observed that with the Mg^{2+} increases, the thermal stability of LDH-(A~E) are gradually reduced. This phenomenon may be due to with the ratio of $Mg^{2+}/(Al^{3+} + Fe^{3+})$ increases, the number of divalent cations increases and the number of tervalent cations decreases, meaning that the density of positive charge decreases, which results that the electrostatic attraction between layer plate and anions becomes weaker, thus the removal of water molecules and interlayer anions becomes easier and the weight loss rate of LDH-(A~E) are gradually increased (19).

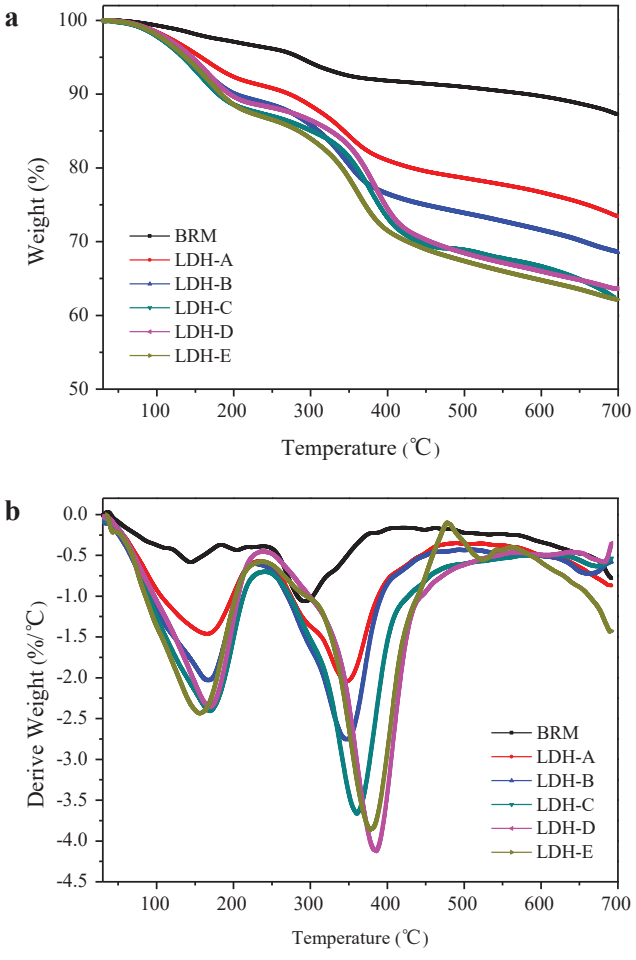

Figure 2: (a) TGA and (b) DTG curves of the BRM and Mg/Al/Fe-LDHs.

3.3 Morphology and dispersion

The morphology and dispersion state of inorganic additives play an important role in affecting the flame retardancy properties of polymer composites. Figure 3a shows the TEM image of BRM. Obviously, the BRM sample exhibits a large number of irregular nanosheets and that aggregates are formed, indicating that BRM is a mixtures of various metal oxides (18). TEM image of LDH-B is shown in Figure 3b, which exhibits a uniform lamellar structure (3). SEM was used to observe the fractured surfaces morphologies of EVA composites to evaluate the dispersion of BRM and LDH-B in the EVA matrix. From Figure 3c, it can be seen that EBRM shows a rough surface with obvious agglomeration structure,

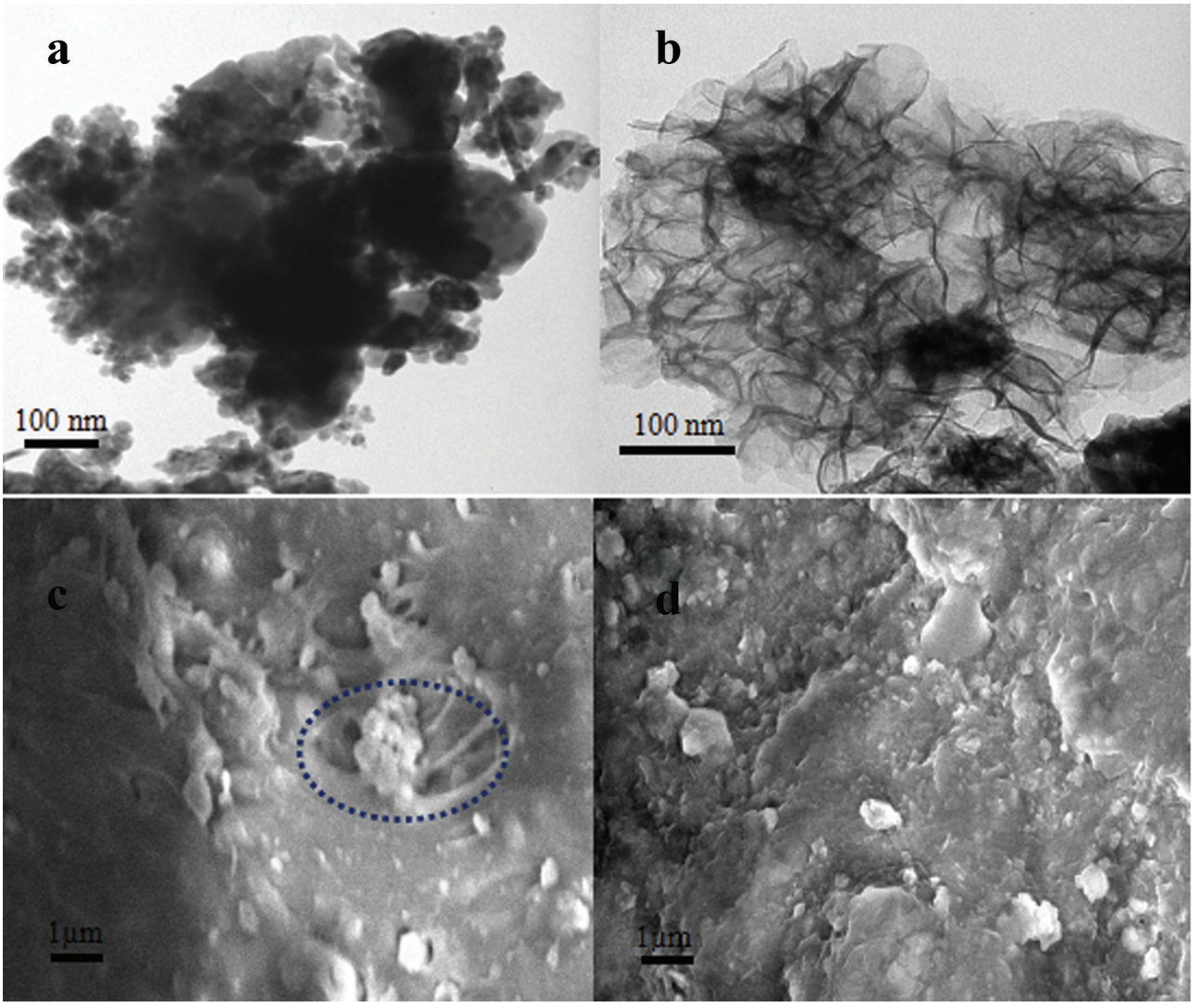

Figure 3: (a) TEM image of BRM, (b) TEM image of LDH-B, (c) SEM image of the fractured surface for EBRM and (d) SEM image of the fractured surface for ELDH2.

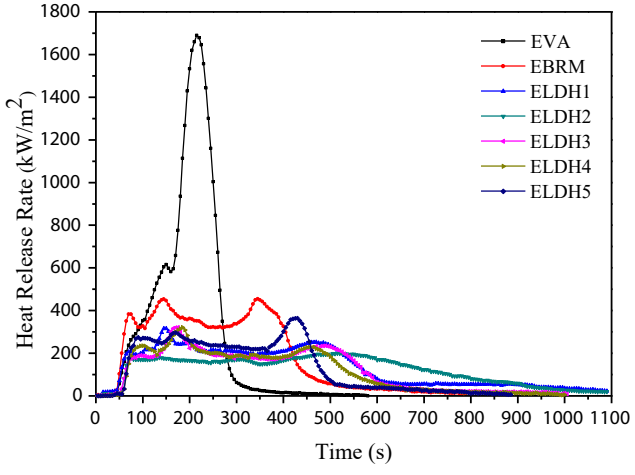

Figure 4: HRR curves of flame retardant EVA composites.

Table 1: Data from cone calorimeter test.

Sample code	PHRR (kW/m²)	THR (MJ/m²)	Time to ignition (s)
EVA	1694.8	179.4	16
EBRM	458.7	143.1	28
ELDH1	316.7	123.9	35
ELDH2	199.2	115.9	47
ELDH3	321.1	121.9	41
ELDH4	321.6	116.7	45
ELDH5	364.7	119.1	44

which indicates that the interfacial interactions between BRM and EVA matrix is so weak that can't be completely stripped. In comparison, LDH-B is

uniformly dispersed in the EVA matrix without a large agglomerate structure.

3.4 Combustion performance of EVA composites

The HRR curves of EVA samples are presented in Figure 4 and the typical data from CCT are shown in Table 1. It can be seen that pure EVA burned fast with a sharp PHRR value of 1694.8 kW/m^2. Compared with EVA, the PHRR value of EBRM is reduced to 458.7 kW/m^2, a decrease by 72.9%. The decrease of PHRR is attributed to char residue layer formation catalyzed by the metal oxide mixtures contained in BRM, which as a protective barrier can slow down heat transfer to the underlying material. Additionally, the HRR curves of ELDH(1~5) are declined significantly compared with that of EVA, especially ELDH2. The PHRR of ELDH2 is 295.9 kW/m^2, a decrease by 88.2% compared with pure EVA. The reduction of PHRR is due to the barrier effect of char residue layer, which effectively limits the release of flammable gases. Moreover, the endothermic decomposition of LDHs reduces the temperature of the polymer system (34,35). At the same time, it can be found from Table 1 that pure EVA is combustible with the time to ignition (TTI) is 16 s. When 50 wt% LDHs were incorporated into EVA, the TTI of ELDH1, ELDH2, ELDH3, ELDH4 and ELDH5 are increased to 35, 47, 41, 45 and 44 s, respectively. The increase of TTI is attributed to the release of water vapor from the decomposition of LDHs, which reduces the temperature of the composite system and dilutes the flammable gas (36).

In order to further study the flame retardancy of EVA composites, the total heat release (THR) for all the samples are investigated. From Figure 5, the THR value of pure EVA is 179.4 MJ/m^2 at 300 s, which is greatly higher than those of other samples. It is easy to see that the incorporation of BRM and LDHs leads to a reduction of THR in all EVA composites. This is because that the 50 wt% of polymer is replaced by inorganic flame retardants, which can release water vapor and promote the formation of char layer, resulting in reducing the transfer of heat into unpyrolysed material (37). It also can be noticed that the THR of composite with BRM is higher than that of composites with the same amount of LDHs, indicating that the latter can improve the flame retardancy of EVA better than the former. It can be illustrated that $Mg(OH)_2$ and $Al(OH)_3$ generated from the thermal decomposition of LDHs offer an enhanced catalytic carbonization capability, and a surface char layer can act as a physical barrier. Additionally, ELDH2 has the lowest THR value, which indicates that ELDH2 sample has the best flame retardant effect.

Figure 6 gives the mass curves of seven samples. Compare with pure EVA (4.8%), there is about 37.5% char residue of EBRM at the end of test. This due to the fact that 50 wt% of combustible polymer is replaced by BRM filler. On the one hand, the metal oxide mixtures contained in BRM have a effect of catalytic carbonization to prevent unpyrolysed material from further combustion; on the other hand, this may be due to the fact that BRM contains non-combustible substances. Additionally, the char residue mass of ELDH(1~5) are higher than EVA. This result demonstrates the incorporation of Mg/Al/Fe-LDHs into EVA matrix is conducive to produce a char residue layer, which acts

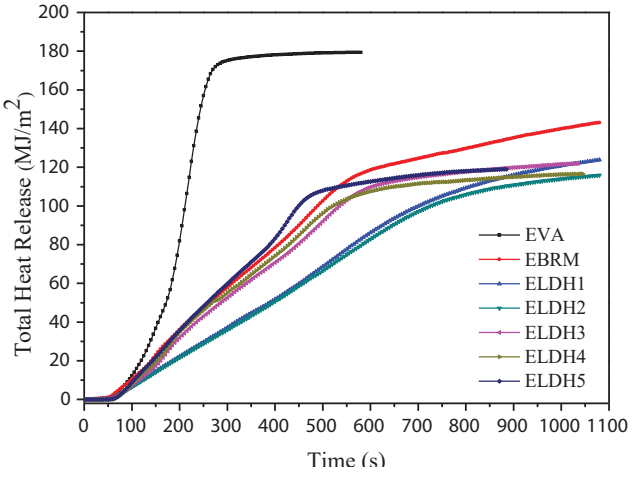

Figure 5: THR curves of flame retardant EVA composites.

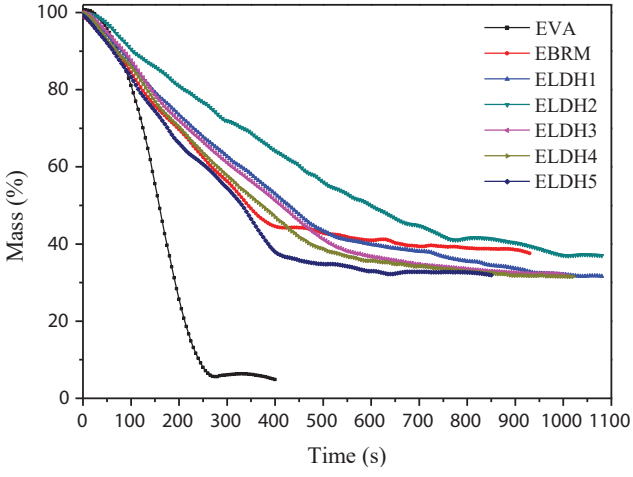

Figure 6: Mass curves of flame retardant EVA composites.

as a physical barrier to slow down the transfer of heat to the underlying material effectively, as a result of reducing the fire hazards of EVA composites. Moreover, it is worth noticing that the mass loss of EBRM obviously lower than ELDH(1~5) after burning completely, this can be explained that the thermal decomposition rate of BRM is lower than LDHs during combustion. The result is also in accordance with the TGA. Taking 40% mass loss as a reference point, it needs 325, 450, 310, 280 and 255 s for the ELDH(1~5), respectively (38). It can be concluded that ELDH2 takes the longest time to get to 40% mass loss, which means that the effect of the flame retardancy is best. These dates further illustrated the HRR and THR results.

In order to further explain the mass loss and observe the morphology of residue, the photographs of seven samples after CCT are shown in Figure 7. As can be seen, pure EVA was burned out, no char residue remaining. For EBRM sample, the surface of char residue becomes compact and rough. This may be due to the catalytic carbonization of the metal oxides contained in the BRM. While for ELDH(1~5) samples, after the introduction of Mg/Al/Fe-LDHs into EVA matrix, the char residue become expanded and smooth, but cracks. This phenomenon may be explained by the fact that the flame retardancy of the polymer is not only related to the char residue layer, but also related to the gases generated during combustion. This expanded and smooth char residue layer can effectively limit heat transfer to the underlying material, thus retarding the combustion process (38). Furthermore, for ELDH(1~5) samples, it can be seen that the ELDH2 sample shows less cracks on the surface of char residue, responding to the smallest mass loss and THR.

3.5 LOI of EVA composites

Figure 8 gives the LOI values of pure EVA and its composites. In general, a higher LOI value represents better flame retardancy (39). The data shows that the pure EVA has the lowest LOI value of 19.0 among all

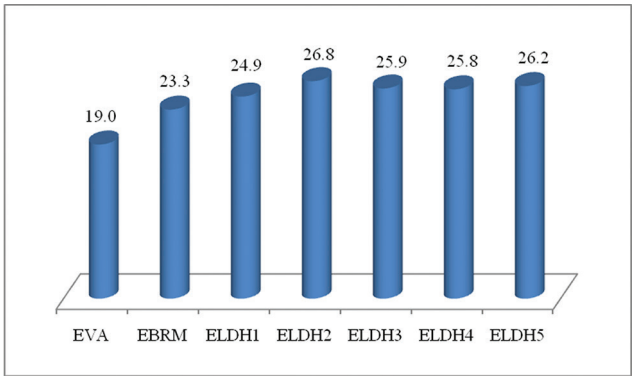

Figure 8: LOI of flame retardant EVA composites.

Figure 7: Photographs of flame retardant EVA composites after cone calorimeter test.

samples. The incorporation of BRM or LDHs into EVA matrix leads the LOI values of EVA composites obviously increased. Compared with EBRM (23.3), the LOI values of ELDH(1~5), increased from 23.3 to 24.9, 26.8, 25.9, 25.8 and 26.2, respectively. These dates demonstrate that the flame retardancy efficiency of the Mg/Al/Fe-LDHs is more excellent than the BRM.

3.6 SDT of EVA composites

Luminous flux can be used to evaluate the amount of smoke production and reflect the smoke density (28). The luminous flux of all samples are presented in Figure 9: (9a) without and (9b) with the application of a pilot flame. It can be seen from Figure 9a that the luminous flux of EBRM sample is higher than EVA before 425 s, while lower than EVA after 425 s. The reason may be explained that BRM can increase the luminous flux value before 425 s by forming some flammable gases, water vapor and less smoke particulates, then smoke particulates begin to reunite and settle after 425 s (38). Compared with EBRM, with the incorporation of LDHs, the smoke density of ELDH(1~5) decreased significantly before 650 s. The reduction of smoke density may be due to the fact that LDHs can generate more water vapor rather than smoke particulates during combustion. Regrettably, the luminous flux of all samples are reduced to zero after 700 s. This can be attributed to the fact that EVA composites eventually generate large amounts of smoke particulates and non-flammable gases under pyrolysis when a pilot flame was not used in the test. From Figure 9b, it can be observed that the luminous flux of pure EVA decreased rapidly in the first 500 s and has the lowest luminous flux value. In the case of EBRM, the luminous flux increased slightly compared with EVA. However, with the incorporation of LDHs, the luminous flux increased greatly. This phenomenon demonstrates the decomposed substance from LDHs, which can completely combustion in the flame and convert into a gas into the gas phase, rather than in the form of smoke particulates. Additionally, it can be noticed that ELDH2 shows the best smoke suppression performance among all samples, with the luminous flux is nearly 95% at the end of test.

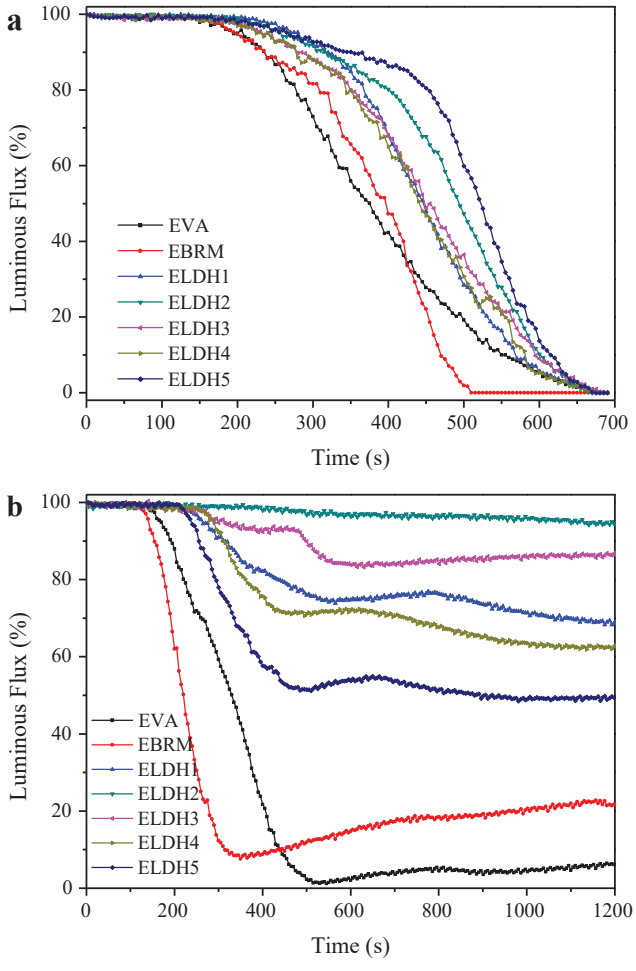

Figure 9: Luminous flux plots of EVA composites: (a) without and (b) with the application of a pilot flame.

3.7 TG-FTIR characterization of EVA composites

Figures 10a and 10b illustrate the TGA and DTG curves of EVA and its composites, respectively. As can be seen, the thermal degradation of EVA involves two stages. The first degradation stage occurs at 250-450°C due to the elimination of acetate side groups (deacetylation), and the second degradation stage occurs at 450-550°C due to the chain scission of ethylene leading to full thermal degradation (3,15). However, both EBRM and ELDH2 samples show similar three thermal degradation stages. The first degradation stage is mainly attributed to the removal of physically adsorbed water molecules in the range of 120-250°C. For EBRM sample, the second and the third stages belong to the dehydroxylation of BRM, the deacetylation and thermal degradation of EVA. The second and third stages of ELDH2 can be attributed to the dehydroxylation and decarburization of LDHs, as well as the fracture decomposition of EVA molecule chains (29). For ELDH2 sample, the degradation rate of the third stage is lower than that of EVA, while significantly higher in the first stage. This may be due to the fact that

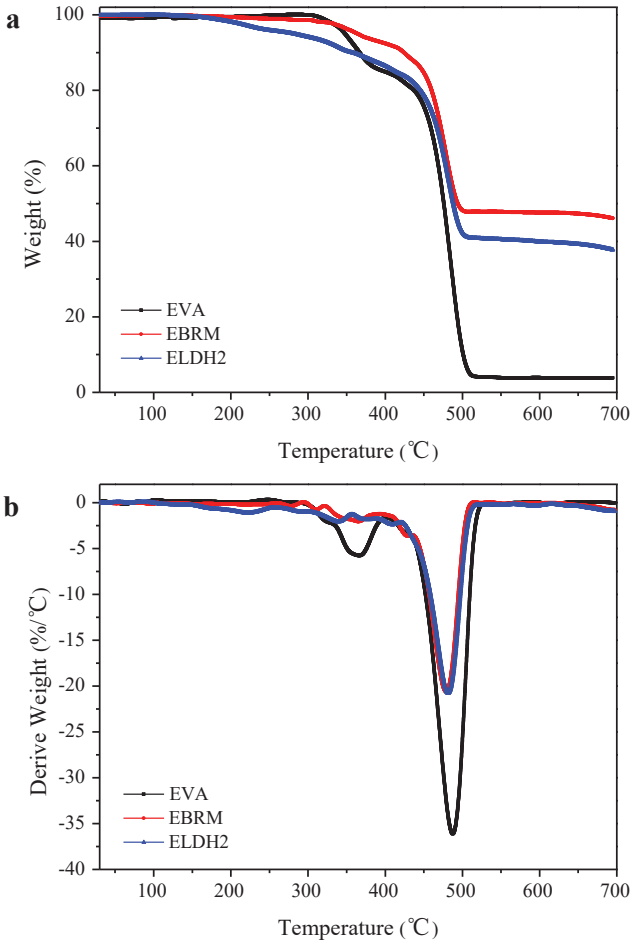

Figure 10: (a) TGA and (b) DTG curves of EVA composites.

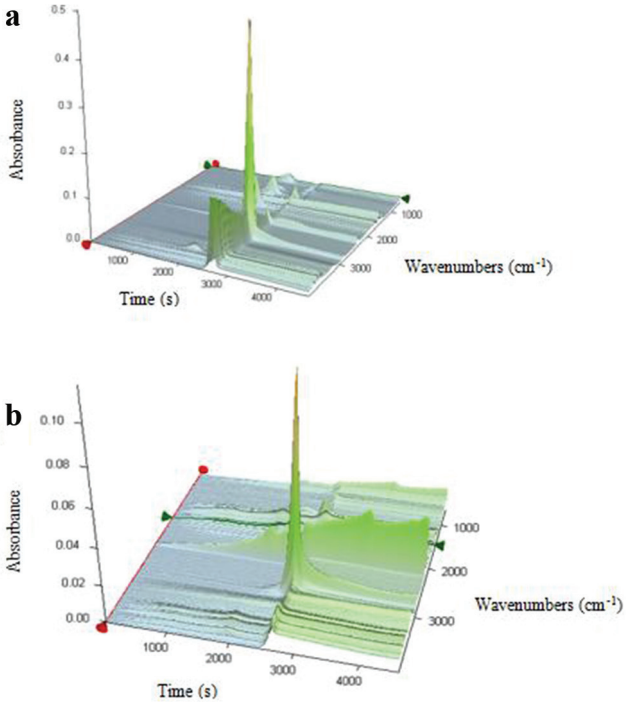

Figure 11: 3D TG-FTIR spectra of pyrolysis products of the composites during the thermal degradation: (a) EVA and (b) ELDH2.

Mg/Al/Fe-LDHs can promote the formation of char residue layer in the thermal degradation process of at low temperature, and the physical barrier can slow down the burning of the matrix material at high temperature. It is worth noting that the char residue of ELDH2 after 700°C are about 37.8%, while there is about 46.1% char residue of EBRM. These date indicate that the decomposition rate of LDHs is higher than that of BRM, meaning that LDHs can absorb more heat than BRM in the thermal degradation process. This result is also in accordance with the TGA of BRM and LDHs.

Figure 11 shows the 3D TG-FTIR spectra of pyrolysis products of EVA and ELDH2 during the thermal degradation. The characteristic bands of the released gas products show at 3400-4000, 2800-3150, 2300-2400, 2250-2300, and 1700-1850 cm^{-1}, attributed to FTIR characteristic bands of H_2O, aliphatic hydrocarbons, CO_2, CO and carboxylic acid, respectively (1,15). This can be explained that the main thermal decomposition products of the EVA composites are the above substances. However, there is a significant difference in the peak intensity and position of the decomposition products of the two samples. In the case of EVA, it decomposes drastically when exposured to heat sources, producing lots of H_2O (3581 cm^{-1}), CO_2 (2360 cm^{-1}), carboxylic acid (1797 cm^{-1}) and aliphatic hydrocarbons (2927 cm^{-1}) in the process of deacetylation and the chain scission of ethylene. Compared with EVA, the intensity of H_2O and CO_2 characteristic bands of ELDH2 are obviously incresed. This due to the fact that more gas phase productions are released during degradation, including H_2O and CO_2.

The FTIR spectra of pyrolysis products of the composites at different temperatures are shown in Figure 12. As we can see, the infrared signal can hardly be detected below 230°C, which indicates that the composites do not decompose or minor decomposition under this temperature. As the temperature increases, the infrared signal of H_2O, CO_2 and CO can be detected. In the case of pure EVA, when the temperature increases to about 340°C, a absorption peak at 1700-1850 cm^{-1} is observed, which reflects the evolution of carboxylic acid. And a absorption peak at 2800-3150 cm^{-1} is observed when the temperature increases to about 460°C, corresponding to the evolution of aliphatic hydrocarbons. Corresponding to the CO_2 absorption peak near 2360 cm^{-1} and the H_2O absorption peak near 3581 cm^{-1}, the intensity are very weak. Moreover, the

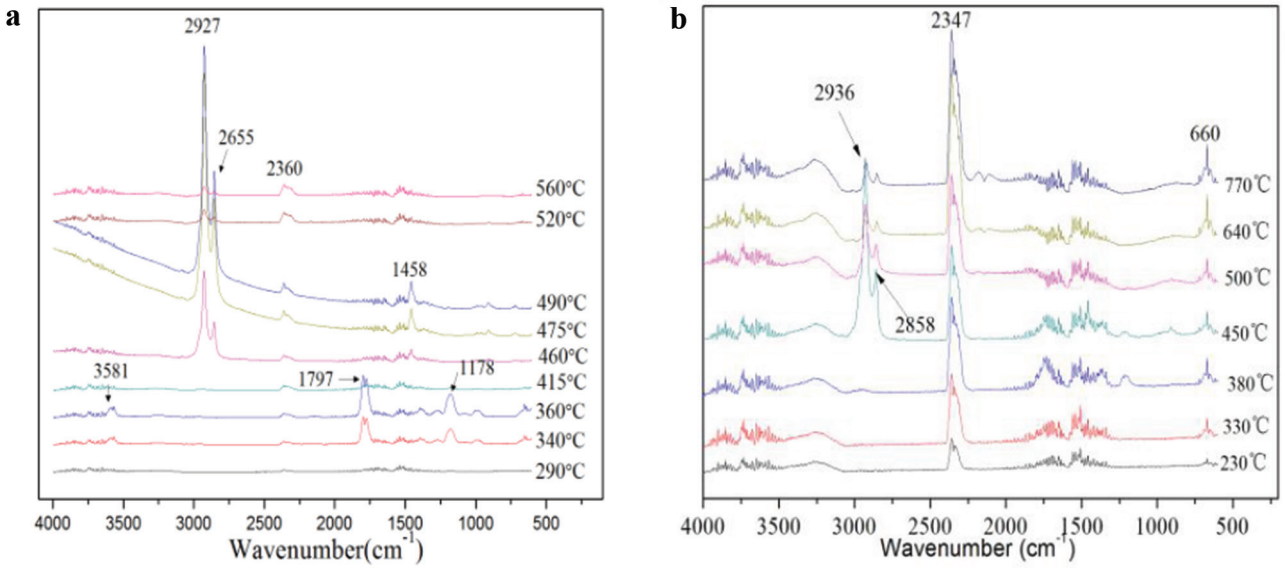

Figure 12: FTIR spectra of pyrolysis products of the composites at different temperatures: (a) EVA and (b) ELDH2.

H_2O absorption peak disappears at around 400°C, and exists in a narrow temperature range. However, compared with EVA, absorption peaks of CO_2 and H_2O for ELDH2 appears at about 230°C, and the intensity and exist temperature range increase significantly. This indicates that the introduction of LDHs into the EVA matrix can promote decomposition of composites to release CO_2 and H_2O at a lower temperature, these non-flammable gases are beneficial for improving flame retardancy, as well as delay the decomposition rate of the composites at a high temperature. In addition, it also can be noticed that the characteristic peak at 2800-3150 cm^{-1} corresponding to aliphatic hydrocarbons decreases significantly. These aliphatic hydrocarbons contain C-H structure, which is the main molecular bond structure of smoke particulates. This indicates that the introduction of LDHs can also reduce the release of toxic and harmful gases.

4 Conclusions

Mg/Al/Fe-LDHs were synthesized successfully by a co-precipitation method based on introducing Mg^{2+} into the BRM suspension. The conclusion can be drawn that synthesis of LDHs based on BRM is a promising way to reduce the hazards of BRM. The TGA results showed that the decomposition rate of LDHs is higher than that of BRM, and the SEM results showed that LDH-B is dispersed well and homogeneously embedded in the EVA matrix. The CCT results showed that LDHs can greatly enhance the flame retardance properties of composites by catalyzing EVA carbonization and prevent unpyrolysed material further combustion. With the incorporation of LDHs, the LOI of EVA composites increased significantly. The SDT results showed that ELDH(1~5) can obviously reduce the smoke production at the end of test with a pilot flame. The TG-FTIR results indicated that the introduction of LDHs can reduce the release of toxic gases and promote decomposition of composites to release CO_2 and H_2O at a lower temperature, as well as delay the decomposition rate of the composites at a high temperature. In conclusion, the LDHs based on BRM will be a effective flame retardant for EVA, which is expected to achieve good economic and environmental benefits.

Acknowledgements: The authors gratefully acknowledge the National Natural Science Foundation of China (No. 51372129, 51572138).

References

1. Bidsorkhi H., Adelnia H., Naderi N., Ethylene vinyl acetate copolymer nanocomposites based on (un)modified sepiolite: Flame retardancy, thermal, and mechanical properties. Polym Composite, 2017, 38, 1302-1310.
2. Nyambo C., Kandare E., Wilkie C., Thermal stability and flammability characteristics of ethylene vinyl acetate (EVA) composites blended with a phenyl phosphonate-intercalated

layered double hydroxide (LDH), melamine polyphosphate and/or boric acid. Polym Degrad Stabil, 2009, 94, 513-520.
3. Wang L., Li B., Zhang X., Effect of intercalated anions on the performance of Ni–Al LDH nanofiller of ethylene vinyl acetate composites. Appl Clay Sci, 2012, 56, 110-119.
4. Zhou K., Gao R., Qian X., Self-assembly of exfoliated molybdenum disulfide (MoS_2) nanosheets and layered double hydroxide (LDH): towards reducing fire hazards of epoxy. J Hazard Mater, 2017, 338, 343-355.
5. Zhou K., Tang G., Gao R., In situ growth of 0D silica nanospheres on 2D molybdenum disulfide nanosheets: towards reducing fire hazards of epoxy resin. J Hazard Mater, 2018, 344, 1078-1089.
6. Zhang J., Kong Q., Wang, D., Simultaneously improving the fire safety and mechanical properties of epoxy resin with Fe-CNTs via large-scale preparation. J Mater Chem A, 2018, 6, 6376-6386.
7. Zhou T., Wu T., Xiang H., Simultaneously improving flame retardancy and dynamic mechanical properties of epoxy resin nanocomposites through synergistic effect of zirconium phenylphosphate and POSS. J Therm Anal Calorim, 2018, 154, 136-144.
8. Zhang J., Kong Q., Yang L., Few layered $Co(OH)_2$ ultrathin nanosheet-based polyurethane nanocomposites with reduced fire hazard: from eco-friendly flame retardance to sustainable recycling. Green Chem, 2016, 18, 3066-3074.
9. Holdsworth A., Horrocks A., Kandola B., The potential of metal oxalates as novel flame retardants and synergists for engineering polymers. Polym Degrad Stabil, 2014, 110, 290-297.
10. Sypaseuth F., Gallo E., Çiftci S., Polylactic acid biocomposites: approaches to a completely green flame retarded polymer. e-Polymers, 2017, 17, 449-462.
11. Ye L., Miao Y., Yan H., The synergistic effects of boroxo siloxanes with magnesium hydroxide in halogen-free flame retardant EVA/MH blends. Polym Degrad Stabil, 2013, 98, 868-874.
12. Pang X., Tian Y., Weng M., Preparation of expandable graphite with silicate assistant intercalation and its effect on flame retardancy of ethylene vinyl acetate composite. Polym Composite, 2015, 36, 1407-1416.
13. Xu G., Cheng J., Wu H., Functionalized carbon nanotubes with oligomeric intumescent flame retardant for reducing the agglomeration and flammability of poly(ethylene vinyl acetate) nanocomposites. Polym Composite, 2013, 34, 109-121.
14. Ye L., Wu Q., Qu B., Synergistic effects and mechanism of multiwalled carbon nanotubes with magnesium hydroxide in halogen-free flame retardant EVA/MH/MWNT nanocomposites. Polym Degrad Stabil, 2009, 94, 751-756.
15. Ye L., Qu B., Flammability characteristics and flame retardant mechanism of phosphate-intercalated hydrotalcite in halogen-free flame retardant EVA blends. Polym Degrad Stabil, 2008, 93, 918-924.
16. Poonoosamy J., Brandt F., Stekiel M., Zr-containing layered double hydroxides: Synthesis, characterization, and evaluation of thermodynamic properties. Appl Clay Sci, 2018, 151, 54-65.
17. Kuila T., Acharya H., Srivastava S., Effect of vinyl acetate content on the mechanical and thermal properties of ethylene vinyl acetate/MgAl layered double hydroxide nanocomposites. J Appl Polym Sci, 2008, 108, 1329-1335.
18. Conterosito E., Gianotti V., Palin L., Facile preparation methods of hydrotalcite layered materials and their structural characterization by combined techniques. Inorg Chim Acta, 2018, 470, 36-50.
19. Qian Y., Li S., Chen X., Synthesis and characterization of LDHs using Bayer red mud and its flame-retardant properties in EVA/LDHs composites. J Mater Cycles Waste, 2015, 17, 646-654.
20. Gao Y., Wang Q., Wang J., Synthesis of highly efficient flame retardant high-density polyethylene nanocomposites with inorgano-layered double hydroxides as nanofiller using solvent mixing method. ACS Appl Mater Inter, 2014, 6, 5094-5104.
21. Han Y., Wu Y., Shen M., Preparation and flame retardancy of polystyrene nanocomposites based on layered double hydroxides. Polym Composite, 2017, 38, 1680-1688.
22. Borra C., Pontikes Y., Binnemans K., Leaching of rare earths from bauxite residue (red mud). Miner Eng, 2015, 76, 20-27.
23. Kong X., Li M., Xue S., Acid transformation of bauxite residue: conversion of its alkaline characteristics. J Hazard Mater, 2017, 324, 382-390.
24. Si C., Ma Y., Lin C., Red mud as a carbon sink: variability, affecting factors and environmental significance. J Hazard Mater, 2013, 244, 54-59.
25. Huang W., Wang S., Zhu Z., Phosphate removal from wastewater using red mud. J Hazard Mater, 2008,158, 35-42.
26. Tor A., Danaoglu N., Arslan G., Removal of fluoride from water by using granular red mud: batch and column studies. J Hazard Mater, 2009, 164, 271-278.
27. Ujaczki É., Zimmermann Y., Gasser C., Red mud as secondary source for critical raw materials–purification of rare earth elements by liquid/liquid extraction. J Chem Technol Biot, 2017, 92, 2683-2690.
28. Li L., Qian Y., Jiao C., Influence of red phosphorus on the flame-retardant properties of ethylene vinyl acetate/layered double hydroxides composites. Iran Polym J, 2012, 21, 557-568.
29. Li L., Qian Y., Jiao C., Synergistic flame retardant effect of melamine in ethylene–vinyl acetate/layered double hydroxides composites. J Therm Anal Calorim, 2013, 114, 45-55.
30. Jia C., Qian Y., Chen X., Flame retardant ethylene–vinyl acetate composites based on layered double hydroxides with zinc hydroxystannate. Polym Eng Sci, 2014, 54, 2918-2924.
31. Vulic T., Reitzmann A., Ranogajec J., The influence of synthesis method and Mg–Al–Fe content on the thermal stability of layered double hydroxides. J Therm Anal Calorim, 2012, 110, 227-233.
32. Nyambo C., Kandare E., Wang D., Wilkie C., Flame-retarded polystyrene: Investigating chemical interactions between ammonium polyphosphate and MgAl layered double hydroxide. Polym Degrad Stabil, 2008, 93, 1656-1663.
33. Zhang H., Wen X., Wang Y., Synthesis and characterization of sulfate and dodecylbenzenesulfonate intercalated zinc–iron layered double hydroxides by one-step coprecipitation route. J Solid State Chem, 2007, 180, 1636-1647.
34. Liu L., Hu J., Zhuo J., Synergistic flame retardant effects between hollow glass microspheres and magnesium hydroxide in ethylene-vinyl acetate composites. Polym Degrad Stabil, 2014, 104, 87-94.
35. Xu W., Zhang B., Xu B., The flame retardancy and smoke suppression effect of heptaheptamolybdate modified reduced graphene oxide/layered double hydroxide hybrids on polyurethane elastomer. Compos Part A-Appl S, 2016, 91, 30-40.

36. Sonnier R., Viretto A., Dumazert L., Fire retardant benefits of combining aluminum hydroxide and silica in ethylene-vinyl acetate copolymer (EVA). Polym Degrad Stabil, 2016, 128, 228-236.
37. Laoutid F., Lorgouilloux M., Bonnaud L., Fire retardant behaviour of halogen-free calcium-based hydrated minerals. Polym Degrad Stabil, 2017, 136, 89-97.
38. Jiao C., Wang H., Li S., Fire hazard reduction of hollow glass microspheres in thermoplastic polyurethane composites. J Hazard Mater, 2017, 332, 176-184.
39. Chen L., Wang Y., A review on flame retardant technology in China. Part I: development of flame retardants. Polym Advan Technol, 2010, 21, 1-26.